Resonance Raman Studies of Cytochrome *c*′ Support the Binding of NO and CO to Opposite Sides of the Heme: Implications for Ligand Discrimination in Heme-Based Sensors†

Colin R. Andrew,*,‡ Edward L. Green,‡ David M. Lawson,§ and Robert R. Eady§

Department of Biochemistry and Molecular Biology, Oregon Graduate Institute of Science and Technology, 20000 NW Walker Road, Beaverton, Oregon 97006-8921, and Department of Biological Chemistry, John Innes Centre, Norwich NR4 7UH, U.K.

Received October 11, 2000; Revised Manuscript Received January 22, 2001

ABSTRACT: Resonance Raman (RR) studies have been conducted on *Alcaligenes xylosoxidans* cytochrome *c*′, a mono-His ligated hemoprotein which reversibly binds NO and CO but not O_2. Recent crystallographic characterization of this protein has revealed the first example of a hemoprotein which can utilize both sides of its heme (distal and proximal) for binding exogenous ligands to its Fe center. The present RR investigation of the Fe coordination and heme pocket environments of ferrous, carbonyl, and nitrosyl forms of cytochrome *c*′ in solution fully supports the structures determined by X-ray crystallography and offers insights into mechanisms of ligand discrimination in heme-based sensors. Ferrous cytochrome *c*′ reacts with CO to form a six-coordinate heme−CO complex, whereas reaction with NO results in cleavage of the proximal linkage to give a five-coordinate heme−NO adduct, despite the relatively high stretching frequency (231 cm^{-1}) of the ferrous Fe−N(His) bond. RR spectra of the six-coordinate CO adduct indicate that CO binds to the Fe in a nonpolar environment in line with its location in the hydrophobic distal heme pocket. On the other hand, RR data for the five-coordinate NO adduct suggest a positively polarized environment for the NO ligand, consistent with its binding close to Arg 124 on the opposite (proximal) side of the heme. Parallels between certain physicochemical properties of cytochrome *c*′ and those of heme-based sensor proteins raise the possibility that the latter may also utilize both sides of their hemes to discriminate between NO and CO binding.

Cytochromes *c*′ (cyt *c*′)[1] are a distinct family of class IIa cytochromes found in the periplasm of certain denitrifying, photosynthetic, methanotrophic, and sulfur-oxidizing bacteria (*1*, *2*). Unlike most *c*-type cytochromes, the heme contains only a single histidine axial ligand resulting in a five-coordinate iron center. In its ferrous state, cyt *c*′ forms reversible complexes with CO and NO but does not generate a stable O_2 adduct. Although the exact role of cyt *c*′ in vivo is unclear, several studies have suggested that NO binding to its heme center may be physiologically relevant (*3*−*7*). In the case of biological denitrification, it has been proposed that cyt *c*′ could capture the obligate NO intermediate and mediate its transfer to NO reductase, thereby helping to suppress potentially toxic levels of free NO which might otherwise be formed (*6*). Interestingly, a recent crystallographic study of cyt *c*′ from the denitrifying bacterium *Alcaligenes xylosoxidans* showed that CO and NO can bind to opposite faces of the heme. Thus, in the 6c-CO adduct the CO binds to the Fe from the distal pocket, whereas in the 5c-NO adduct the NO adopts an unprecedented proximal Fe coordination (*8*). Not only do the NO and CO adducts of cyt *c*′ represent the first structurally characterized example of exogenous ligand binding to the Fe from both sides of a protein heme cofactor, the 1.35 Å resolution structure of the cyt *c*′-NO complex is the first ever reported for a 5c-NO adduct within a hemoprotein. The novel features of ligand binding to the Fe center of cyt *c*′ are of potential relevance to the mechanisms of heme-based sensors. These proteins, which include soluble guanylate cyclase (sGC), FixL, and CooA, play a central role in regulating important biological processes by sensing changes in the concentrations of NO, O_2, and CO, respectively (*9*). In each case, it is thought that binding of the target ligand to the heme center leads to a conformational change within the protein which acts as a switch to generate a cellular response. Important questions relate to the mechanisms of ligand discrimination and signal transduction in heme-based sensors. The crystallographic data of cyt *c*′, showing that CO and NO can bind to opposite sides of the heme, have implications for ligand-selective responses in sGC and CooA, as well as for the nature of

† This work was supported by NIH Grant GM 34468 to Professor Thomas M. Loehr. R.R.E. and D.M.L. are funded by the BBSRC as part of the competitive strategic grant to the John Innes Centre.

* To whom correspondence should be addressed. Fax: (503) 748-1464. E-mail: candrew@bmb.ogi.edu.

‡ Oregon Graduate Institute of Science and Technology.

§ John Innes Centre.

[1] Abbreviations: 5c and 6c, five-coordinate and six-coordinate, respectively; HS and LS, high-spin and low-spin electronic configurations of iron, respectively; cyt *c*′, cytochrome *c*′; cyt *c*′-NO_{5c}, five-coordinate NO adduct of ferrous cyt *c*′; cyt *c*′-CO, six-coordinate CO adduct of ferrous cyt *c*′; sGC_1, soluble guanylate cyclase reconstituted with heme; sGC_2, soluble guanylate cyclase isolated with heme intact; CooA, CO oxidation activator; FixL*, soluble truncated form of O_2-sensing protein; FixLN, heme domain of FixL*; Mb, myoglobin; HRP, horseradish peroxidase; CCP, cytochrome *c* peroxidase; TPP, tetraphenylporphyrin.

10.1021/bi0023652 CCC: $20.00
Published on Web 03/06/2001

conformational changes induced in these proteins upon heme−ligand binding.

X-ray crystal structures of the ferrous and oxy forms of FixL show that activation is associated with flattening of the porphyrin ring upon O_2 binding to the distal side of the His-ligated heme (*10*, *11*). In the case of CooA, a recent crystallographic study of the ferrous form has revealed a 6c-heme with novel axial ligation from the nitrogen of the N-terminal proline as well as a histidine residue (*12*). Since no crystallographic data have been published to date for sGC or for ligand adducts of CooA, structural investigations of these heme-based sensor proteins and their activation mechanisms have relied heavily on spectroscopic measurements. A particularly powerful technique for investigating the structures of heme centers in proteins is resonance Raman (RR) spectroscopy, which yields information on the Fe spin state, coordination geometry, and axial-ligand bond strengths (*13*). In the case of CooA the ferrous heme center has been shown to be 6c-LS (*14*), while for sGC there are two types of enzyme depending on which isolation procedure is used: sGC_1, which is 6c-LS in its Fe(II) state (*15*, *16*), and sGC_2, which is 5c-HS (*17*, *18*). Both versions of sGC, as well as CooA, react with CO and NO to form 6c and 5c adducts, respectively (*15*, *16*−*19*).

For hemes complexed with CO or NO, RR spectra can also provide information on the extent of back-bonding, which in turn can be used to determine the electrostatic environment of the heme pocket. In this study, we report Soret excitation RR investigations of *A. xylosoxidans* cyt *c*′ in its ferrous state together with its complexes with CO and NO. Our RR data of the 6c-CO and 5c-NO adducts of cyt *c*′ are consistent with exogenous ligand binding in the distal and proximal heme pockets, respectively, thus agreeing with the structures determined by X-ray diffraction in the crystalline state. The implications of the cyt *c*′ RR data to the ligand adducts of heme-based sensors are discussed.

MATERIALS AND METHODS

A. xylosoxidans cyt *c*′ was purified using procedures similar to those described previously (*20*, *21*). Heme concentrations for RR experiments (50−100 μM) were determined from electronic absorption measurements using previously reported absorptivities (*22*). Reduction to the ferrous state was achieved by the addition of an ∼10-fold excess of freshly prepared sodium dithionite solution to an argon-purged sample. ^{12}CO (CP grade, Air Products) and ^{13}CO (99% ^{13}C, Cambridge Isotope Laboratory) adducts were prepared by injecting ∼1 mL of gas through a septum-sealed capillary containing argon-purged reduced protein (∼20 μL). NO adducts were prepared by equilibrating ∼20 μL of reduced protein for 20 min with ∼1 mL of ^{14}NO (Aldrich) or ^{15}NO (98% ^{15}N, Cambridge Isotope Laboratory) gas which had been bubbled through 0.1 M KOH solution to remove higher oxides of nitrogen.

Resonance Raman spectra were recorded on a custom McPherson 2061/207 spectrograph (set to 0.67 m) equipped with a Princeton Instruments liquid N_2-cooled (LN-1100PB) CCD detector. Kaiser supernotch filters were used to attenuate Rayleigh scattering. Excitation wavelengths were provided by the 413.1 nm line of a Kr ion laser (Innova 302) or the 441.6 nm line of a He−Cd laser (Liconix 4240NB).

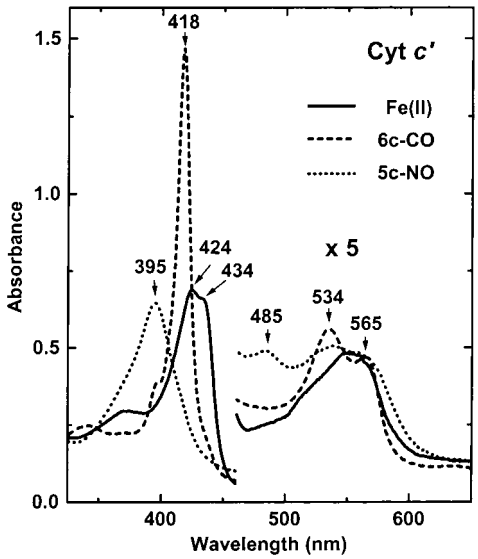

FIGURE 1: Electronic absorption spectra of solutions of ferrous cyt *c*′ (—), cyt *c*′-CO (---), and cyt *c*′-NO_{5c} (•••). The sample contained 7 μM heme and 50 mM sodium phosphate buffer at pH 7.0, 25 °C.

Room temperature spectra were collected in a 90° scattering geometry for periods of 10−20 min using low laser powers (<0.5 mW) together with a reciprocating translation stage to minimize photochemistry. Higher laser power and a backscattering geometry were used for frozen samples. Frequencies were calibrated relative to indene, aspirin, and CCl_4 as standards and are accurate to ±1 cm^{-1}. Optical absorption spectra of RR samples in their capillary cells were checked before and after laser illumination using a Perkin-Elmer Lambda 9 spectrophotometer (*23*).

RESULTS

Ferrous Cyt c′. The UV−vis absorption spectrum of ferrous cyt *c*′ is dominated by a split Soret band with maxima at 372, 424, and 434 (sh), together with a broad $\alpha\beta$ envelope centered near 550 nm (Figure 1). Excitation at 413.1 nm yields RR frequencies characteristic of a 5c-HS Fe(II) heme (Figure 2A and Table 1) including the porphyrin marker bands ν_4 (1351 cm^{-1}), ν_3 (1469 cm^{-1}), and ν_{10} (1603 cm^{-1}). It is noted that the band at 1577 cm^{-1}, which we assign as the ν_2 mode, has an unusually high frequency compared to those of other 5c-HS hemes—a trend also observed in the CO and NO adducts (vide infra). The RR frequencies are similar to those previously reported for *A. xylosoxidans* cyt *c*′ with Q-band excitation (*24*), as well as to a range of cyt *c*′s from photosynthetic bacteria (Table 1) (*25*−*28*).

Figure 3A shows the low-frequency RR spectrum of ferrous cyt *c*′ obtained with 413.1 nm excitation including contributions from the ν_7 mode at 682 cm^{-1} together with a band at 231 cm^{-1} which we assign as the Fe−N(His) stretch, ν(Fe−His). The assignment of the ν(Fe−His) is supported by its increase in relative intensity upon changing the excitation wavelength to 441.6 nm (Figure 3B) and to its disappearance in the CO and NO adducts (vide infra). Similar ν(Fe−His) frequencies have been reported for cyt *c*′s from the photosynthetic bacteria *Rhodospirillum molischianum* (228 cm^{-1}), *Rhodobacter sphaeroides* (231 cm^{-1}), and *Chromatium vinosum* (231 cm^{-1}) (*27*, *28*). No change in the appearance of either the low-frequency or high-frequency

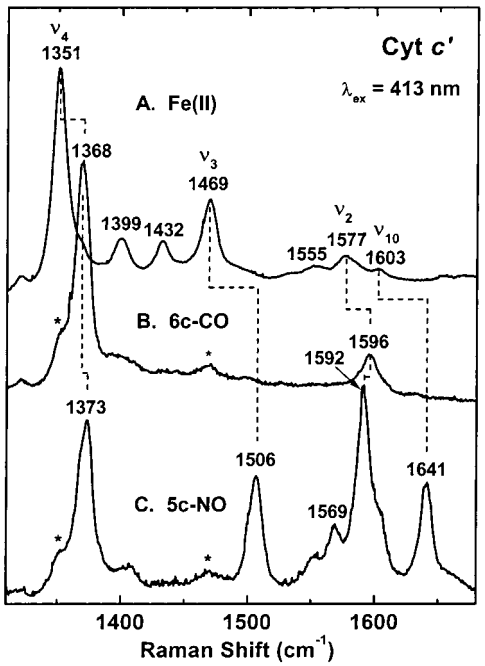

FIGURE 2: High-frequency region of RR spectra of ferrous cyt *c*′ (A), together with its 6c-CO adduct (B) and 5c-NO adduct (C). Spectra were obtained from solutions of ~100 μM heme in 50 mM sodium phosphate buffer, pH 7, at room temperature using 413.1 nm excitation (10 mW for the reduced sample or 0.3 mW for the CO and NO complexes). Asterisks denote minor contributions from ferrous cyt *c*′ produced by photodissociation in the laser beam.

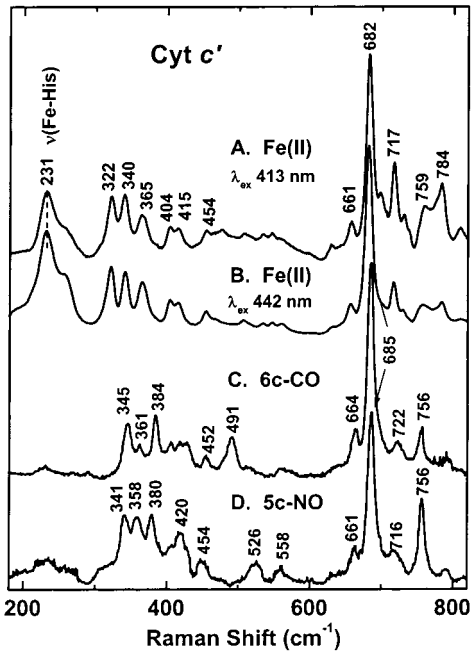

FIGURE 3: Low-frequency region of RR spectra of ferrous cyt *c*′ (A and B), together with its 6c-CO adduct (C) and 5c-NO adduct (D). Spectra were obtained as described in Figure 2, except for (B) which was obtained using 441.6 nm excitation (5 mW).

Table 1: Resonance Raman Frequencies (cm^{-1}) for Ferrous Cyt *c*′s and Other Five-Coordinate Hemoproteins[a]

	ν_4	ν_3	ν_2	ν_{10}	ν(Fe−His)	ref
A.x. cyt *c*′	1351	1469	1577	1603	231	this work
A.x. cyt *c*′	1353	1471	1575	1604	nr	*24*
R.m. cyt *c*′	1354	1468	1573	1604	228	*28*
R.s. cyt *c*′	1354	1468	1573	1604	231	*28*
R.p. cyt *c*′	1355	1475	nr	1609	nr	*25*
R.r. cyt *c*′	1355	1472	nr	1609	nr	*26*
C.v. cyt *c*′	1352	1469	1577	nr	231	*27*
Mb	1357	1473	1563	1607	220	*48*
FixL*	1355	1470	1558	nr	209	*49*
sGC_2	1358	1471	1562	1606	204	*17*
HRP	1359	1473	1567	1605	244	*50*

[a] Abbreviations: *A.x.*, *Alcaligenes xylosoxidans*; *R.m.*, *Rhodospirillum molischianum*; *R.s.*, *Rhodobacter sphaeroides*; *R.p.*, *Rhodopseudomonas palustratis*; *R.r.*, *Rhodospirillium rubrum*; *C.v.*, *Chromatium vinosum*; nr, not reported.

RR spectrum of ferrous *A. xylosoxidans* cyt *c*′ was detected over the pH range 3.1−8.8 (data not shown).

The relatively high frequency of the ν(Fe−His) mode of cyt *c*′ compared to that of most other 5c-HS hemes (Table 1) is suggestive of an increased ligand field strength due to significant imidazolate character in the side chain of the proximal histidine. As well as the electronegativity of the His ligand, it has also been proposed that the frequency of the ν(Fe−His) vibration depends on the dihedral angle, ϕ, between the imidazole plane and the nearest N(pyrrole)−Fe−N(pyrrole) axis, the value of which differs markedly among hemoproteins (*28*−*30*). A study in which values of ν(Fe−His) were plotted against ϕ revealed an apparently linear negative correlation such that ν(Fe−His) downshifted by approximately 0.5 cm^{-1}/deg (*28*). The same study showed that anionic-like histidine coordination (as exemplified by peroxidases) can be distinguished from the more neutral form of histidine ligation (e.g., Mb) on account of the correlation line being displaced ~30 cm^{-1} toward higher ν(Fe−His) values. Analysis of the recent X-ray crystal structures of *A. xylosoxidans* cyt *c*′ reveals that the imidazole ring of His 120 is oriented such that ϕ is ~33° in both the ferrous and ferric states (*31*). This, together with the ν(Fe−His) frequency of 231 cm^{-1}, places *A. xylosoxidans* cyt *c*′ on the same correlation line as that of peroxidases with imidazolate ligation. A similar conclusion was reached by Desbois and co-workers for *R. molischianum* cyt *c*′ using the ν(Fe−His) frequency of 228 cm^{-1} together with the ϕ value of ~43° taken from the structure of the ferric state (*28*). Thus, according to the model described above, the lower ν(Fe−His) frequency of *A. xylosoxidans* cyt *c*′ (231 cm^{-1}) compared to that of a peroxidase such as CCP (247 cm^{-1}) is a consequence of the different ϕ values of ~33° and ~7°, respectively.

In the case of peroxidases, the anionic nature of the proximal His ligand can be ascribed to a polarized H-bond between the N_δ and the carboxylate(O) of an Asp residue. However, for ferrous cyt *c*′, the apparent imidazolate character of the proximal histidine is somewhat surprising given the absence of carboxylate (or even carbonyl) groups within H-bonding distance (*8*). The crystal structure of *A. xylosoxidans* cyt *c*′ shows that the only H-bond involving His 120 is with a solvent-accessible water molecule—an interaction which by itself is unlikely to lead to imidazolate character. Deprotonation of the proximal His has also been proposed to occur in ferric cytochromes *c*′ in order to account for the change in spin state at moderately alkaline pH (pK_a 7−9) (*32*). It has been suggested that negative charge on the proximal ligand in cyt *c*′ could be stabilized ionically by a nearby positively charged residue (*2*, *28*, *32*, *33*). As with *A. xylosoxidans* cyt *c*′, where His 120 is closely associated with Arg 124, crystallographic data from other

Table 2: Resonance Raman and Infrared Frequencies (cm^{-1}) of the Six-Coordinate CO Adducts of Cyt *c′* and Other Hemoproteins

	ν_4	ν_2	ν_{10}	ν(Fe−CO)	δ(Fe−CO)	ν(C−O)	ref
cyt *c′* [a]	1368	1596	no[c]	491	572	1966	this work
cyt *c′* [b]	1371	1591	no	492	565	1978	*27*
sGC_2	1369	1578	1627	473	564	1987	*17*, *18*, *51*
sGC_1	1371	1582	1627	497	574	1959	*15*, *16*
CooA	1371	1579	1622	487	572	1983	*14*
FixL*	nr[d]	nr	nr	498	572	1962	*52*
Mb	1372	1587	1637	512	577	1944	*53*

[a] Data from *A. xylosoxidans*. [b] Data from *C. vinosum*. [c] Not observed. [d] Not reported.

cytochromes *c′* show that in each case the proximal His is located close to either a Arg or Lys residue.

Carbonyl Adduct. Addition of CO to ferrous cyt *c′* generates absorption bands at 418, 534, and 565 nm, characteristic of a hexacoordinate heme−CO complex with an axial histidine ligand (Figure 1). Excitation at 413.1 nm yields the RR spectrum of the CO adduct (Figures 2B and 3C) together with a minor contribution from 5c ferrous cyt *c′* due to the photolabile nature of the Fe−CO bond. In the high-frequency region (Figure 2B) the predominant RR features of the CO adduct are the ν_4 oxidation state marker band at 1368 cm^{-1}, its relatively high frequency indicative of π-back-bonding from the Fe(II) to the CO ligand, and the ν_2 mode at 1596 cm^{-1}. As with ferrous cyt *c′*, the frequency of ν_2 in the CO adduct is unusually high compared to other hemoproteins (Table 2).

More detail concerning the proximal and distal heme environments of the CO adduct is obtained from the identification and analysis of vibrations within the Fe−CO moiety. Substitution of ^{12}CO with ^{13}CO produces frequency shifts in the peaks at 491 (−4), 571 (−10), and 1966 (−46) cm^{-1}, consistent with their assignment as ν(Fe−CO), δ(Fe−CO), and ν(CO), respectively, as shown in Figure 4. The data are similar to the previously reported ν(Fe−CO) and ν(CO) frequencies for *C. vinosum* cyt *c′* which occur at 492 and 1978 cm^{-1}, respectively (Table 2) (*27*). Analysis of the relative ν(Fe−CO) and ν(CO) values by means of a back-bonding correlation diagram (Figure 5) yields two pieces of information. First, it can be seen that the cyt *c′* data fall on the line corresponding to CO adducts in which the proximal ligand is neutral histidine with a protonated N_δ. Second, the position of the cyt *c′* data along the correlation line is typical of a CO ligand in a nonpolar environment.

The environment of the CO ligand deduced from the RR data is fully consistent with the X-ray crystal structure of the carbonyl adduct which shows that the Fe-bound CO is surrounded by hydrophobic residues in the distal pocket. Since the RR data indicate that the proximal histidine is neutral in the CO adduct but highly electronegative in the ferrous state, it appears that CO binding to cyt *c′* is accompanied by protonation of the His 120 N_δ, possibly due to the loss of electrostatic stabilization as it moves away from Arg 124 (*8*). It is noted that the X-ray crystal structure of the carbonyl adduct shows a second CO molecule H-bonded directly to the N_δ atom of His 120—an interaction which may be likened to the situation in many hemoproteins where the proximal histidine forms a H-bond with a main-chain carbonyl group. Although this second CO may be a photodissociated ligand trapped in the crystal at low temperature, it nevertheless supports the existence of a protonated histidine in the carbonyl adduct.

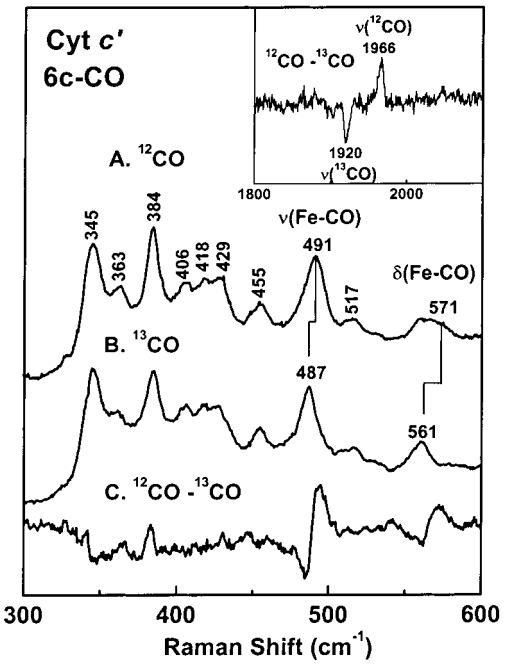

FIGURE 4: Low-frequency RR spectra of ferrous cyt *c′* complexed with ^{12}CO (A) and ^{13}CO (B), together with the ^{12}CO − ^{13}CO difference spectrum (C). The inset shows the ^{12}CO − ^{13}CO difference spectrum in the high-frequency region. Spectra were obtained under the conditions described in Figures 2 and 3.

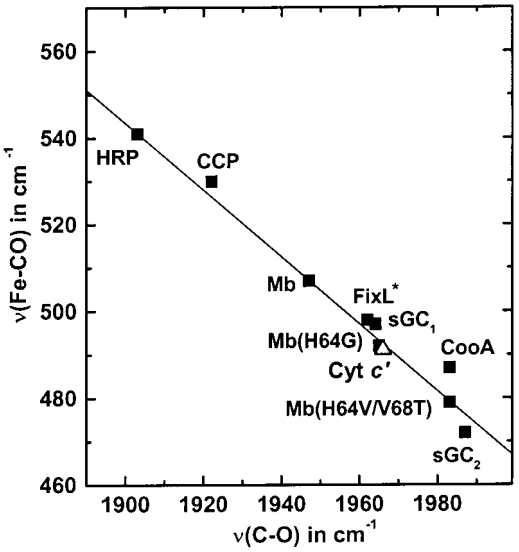

FIGURE 5: Plot of observed ν(Fe−CO) vs ν(C−O) frequencies for six-coordinate CO adducts of ferrous hemoproteins. The solid line indicates the back-bonding correlation for proximal neutral imidazole ligation. Data obtained in the present study for cyt *c′* are denoted by an open triangle. Solid squares represent data points of other CO adducts (see Abbreviations) taken from Table 1, with the addition of HRP (*54*), CCP (*55*), Mb(H64G) (*56*), and Mb(H64V/V68T) (*57*).

Nitrosyl Adduct. Equilibration of ferrous cyt *c′* with excess NO results in an end product with absorption bands at 395 and 485 nm, characteristic of a 5c-NO heme (Figure 1). The absorption spectrum is similar to that previously reported by Iwasaki et al. (*34*). Further evidence for a 5c-NO heme is provided by RR spectra at 413.1 nm excitation (Figures 2C and 3D). The elevated frequencies of the porphyrin

Table 3: Resonance Raman Frequencies (cm^{-1}) for Five-Coordinate Nitrosyl Adducts of Cyt *c′* and Other Hemoproteins

protein	temp (°C)	ν_4	ν_3	ν_2	ν_{10}	ν(Fe−NO)	ν(N−O)	ref
cyt *c′*	RT[a]	1373	1506	1592	1641	526	1661	this work
sGC_2	20	1375	1509	1583	1646	521	1681	*18*
sGC_2	10−20	1375	1509	1584	1646	525	1677	*17*
sGC_1	RT	1375	1508	1584	1645	520	no[b]	*15*
sGC_1	nr[c]	1374	1508	1584	1644	no	1660	*16*
CooA	nr	1376	1506	1582	1641	523	1672	*19*
FixL*	20	nr	1509	nr	1646	525	1675	*38*
FixLN	20	nr	1509	nr	1646	525	1676	*38*
FixLN	−45	nr	1509	1583	1646	526	1664, 1676	*38*
H93Y Mb	nr	nr	nr	nr	nr	524	1672	*16*

[a] RT, room temperature. [b] Not observed. [c] Not reported.

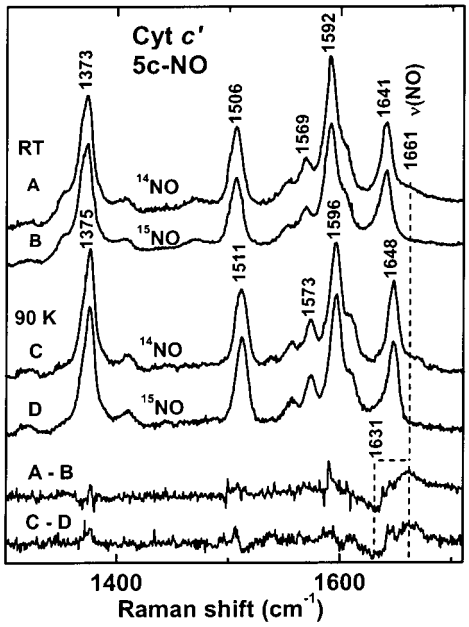

FIGURE 6: Effect of isotopic substitution and temperature on the high-frequency RR spectrum (413.1 nm excitation) of the five-coordinate NO adduct of ferrous cyt *c′*: (A) ^{14}NO, room temperature; (B) ^{15}NO, room temperature; (C) ^{14}NO, 90 K; (D) ^{15}NO, 90 K. The (A) − (B) and (C) − (D) difference spectra are expanded by a factor of 2. Experimental conditions are as described in Figure 2.

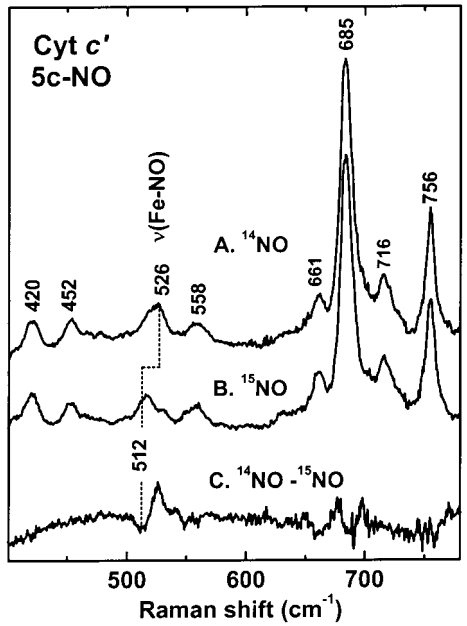

FIGURE 7: Low-frequency RR spectrum (413.1 nm excitation, room temperature) of the five-coordinate NO adduct of ferrous cyt *c′* complexed with ^{14}NO (A) and ^{15}NO (B). The ^{14}NO − ^{15}NO difference spectrum (C) is expanded by a factor of 1.7. Experimental conditions are as described in Figure 2.

marker bands, ν_3 (1506 cm^{-1}) and ν_{10} (1641 cm^{-1}), are a feature of hemes with a 5c-NO geometry (Table 3), while the unusually high frequency of the ν_2 mode (1592 cm^{-1}) compared to other 5c-NO hemes continues the trend apparent in the RR spectra of the unligated Fe(II) state as well as the CO adduct (Tables 1 and 2). Isotopic substitution of ^{14}NO with ^{15}NO allows the axial-ligand stretching modes, ν(Fe−NO) and ν(N−O), to be assigned from their frequency shifts at 526 (−14) and 1661 (−30) cm^{-1}, respectively (Figures 6 and 7). These ν(Fe−NO) and ν(N−O) frequencies for cyt *c′* are in the range expected for a 5c-Fe(II)NO heme, as opposed to 6c-Fe(II)NO hemes which exhibit frequencies near 550 and 1600 cm^{-1}, respectively (*35*). A feature of the 5c-NO cyt *c′* adduct at room temperature is its tendency to photodissociate in the laser beam as judged by the appearance of RR bands characteristic of the unligated ferrous state with laser powers >0.5 mW. Since the loss of NO in this manner is expected to initially lead to a four-coordinate heme, the observation of the 5c ferrous cyt *c′* spectrum implies that the proximal histidine ligand reattaches itself faster than the vibrational time scale.

What structural information can be deduced from RR spectra of the 5c-NO cyt *c′* adduct and how does this relate to the X-ray crystal structure? For example, do plots of ν(Fe−NO) vs ν(N−O) predict the electrostatic environment of the heme pocket in a manner analogous to the back-bonding correlations employed for CO−heme complexes? A recent RR study of synthetic 5c-Fe(II)NO porphyrins containing different electron-donating and electron-withdrawing substituents showed that there is indeed an inverse correlation of ν(Fe−NO) vs ν(N−O), which reflects the degree of back-bonding from the Fe(II) to the NO ligand, as shown in Figure 8 (*36*). For example, the electron-donating 4-OCH_3 derivative of TPP allows for increased back-bonding relative to underivatized TPP resulting in a higher ν(Fe−NO) and decreased ν(N−O) frequency, whereas the opposite effect is observed for electron-withdrawing halogen substituents. When the RR data from 5c-NO hemoproteins are included on the same correlation diagram (Figure 8), it can be seen that the data point for cyt *c′* falls in the upper left region close to that of the 4-OCH_3 derivative of TPP. Since this region of the correlation plot is associated with relatively strong back-bonding, it suggests that the NO ligand in cyt *c′* is bound in a positively polarized (rather than neutral)

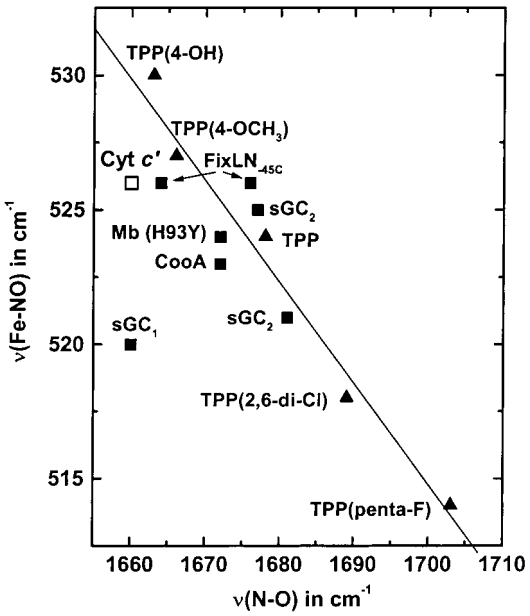

FIGURE 8: Plot of observed ν(Fe−NO) vs ν(N−O) frequencies for five-coordinate NO adducts of ferrous hemoproteins and metalloporphyrin analogues. Data points for protein NO adducts (see Table 3) are denoted by solid squares except for cyt *c*′, which is marked by a open square. Solid triangles correspond to data from phenyl-modified derivatives of Fe(II)TPP(NO) taken from ref *36*.

environment. This interpretation is consistent with the crystal structure which shows that NO binds close to the guanadinium group of Arg 124 on the *proximal* side of the heme. It is noted that the link between increased back-bonding and the presence of an Arg residue in the heme pocket has precedence in the CO adducts of CCP and HRP (Figure 5) (*37*).

Since cyt *c*′ is the only hemoprotein whose 5c-NO adduct has been crystallographically characterized, it remains to be seen how different heme pocket environments affect the 5c-NO RR frequencies. It has been proposed that in hemoprotein nitrosyl adducts the geometry of the Fe−NO moiety is easily perturbed by the heme pocket, leading to deviations in the ν(N−O) vs ν(Fe−NO) correlations. For example, a study of 6c-NO adducts from a series of myoglobin mutants found that changes in the polarity of the distal pocket affected the ν(NO) frequency but had negligible effect on ν(Fe−NO) (*35*). On the other hand, alterations in the steric hindrance of the distal pocket influenced ν(Fe−NO) but not ν(NO)—behavior the authors attributed to changes in the Fe−NO tilting angle. Spiro and co-workers have proposed that Fe−N−O angles of less than 140° give rise to decreased frequencies for the ν(N−O) and/or ν(Fe−NO) mode, causing the data points to fall below the correlation line defined by synthetic NO porphyrins (*16*). Using this argument, the authors have put forward the suggestion that sGC_1 contains a substantially distorted Fe−NO geometry. Together with sGC_1, cyt *c*′ has one of the lowest reported ν(NO) frequencies for a 5c-NO hemoprotein (Table 3). However, cyt *c*′ has a significantly higher ν(Fe−NO) frequency than sGC_1, which places it closer to the back-bonding correlation line (Figure 8). This fact, together with the fairly typical Fe−N−O angle of ∼128° observed in the X-ray crystal structure, argues against angular distortion as the source of the low ν(NO) frequency in cyt *c*′.

Two equally populated conformations for the bound NO are observed in the cyt *c*′-NO_{5c} crystal structure: NO 2 which forms a H-bond to Arg 124 and NO 1 which does not (*8*). RR measurements carried out in the present study on cyt *c*′-NO_{5c} in D_2O buffer did not reveal any deuterium-sensitive vibrations (data not shown). However, on the basis of their different electrostatic environments, the two conformers might be expected to give rise to different ν(N−O) values with NO 2 occurring at a lower frequency than NO 1. The broad nature of the ν(N−O) band observed in the present RR study may reflect the existence of multiple conformers of the Fe−N−O moiety. Previous RR studies on the 5c-NO adduct of FixLN have detected multiple ν(N−O) vibrations at 1664 and 1676 cm^{-1} at low temperature (*38*). In the case of cyt *c*′-NO_{5c}, cooling from room temperature to 90 K produces changes in the RR frequencies of several of the porphyrin vibrations but does not lead to the resolution of ν(N−O) components (Figure 6C). Nevertheless, recent FTIR studies of *A. xylosoxidans* cyt *c*′-NO_{5c} in D_2O buffer show an ν(N−O) absorbance band resolved into a major peak at 1656 cm^{-1} and weaker shoulder near 1678 cm^{-1} (*39*). Since the RR spectrum is not D_2O sensitive, the difference in the apparent ν(N−O) band positions between the FTIR and RR spectra may be due to the relative sensitivity of each technique toward Fe−N−O conformers with different polarization properties.

In summary, the different heme-pocket environments suggested by the RR data of the 6c-CO and 5c-NO adducts are consistent with CO and NO binding to opposite sides of the heme in solution. The fact that the cyt *c*′-CO RR data suggest a neutral environment for the exogenous ligand is in accord with the X-ray crystal structure which shows CO binding in the hydrophobic distal pocket. In contrast, the RR frequencies of the 5c-NO adduct suggest that the NO ligand is influenced by a positively polarized environment, consistent with the crystal structure which reveals an Fe−NO conformer H-bonded to Arg 124 on the proximal side of the heme.

DISCUSSION

The present RR studies of *A. xylosoxidans* cyt *c*′ have implications for CO and NO binding to the heme-based sensors sGC and CooA. In common with *A. xylosoxidans* cyt *c*′, the ferrous hemes of sGC and CooA react with CO to form 6c complexes, whereas with NO they prefer a 5c geometry. The difference in heme coordination number between the NO and CO adducts has been linked to the selective functional responses of sGC and CooA toward these two gases. Thus, NO binding to sGC has been found to increase basal enzyme activity by a factor of 50−200 whereas CO binding has only a 1.4−4-fold effect (*16*, *18*, *40*, *41*). Conversely, CooA is activated by CO but not by NO (*19*).

The origin of the different heme coordination geometries for NO and CO stems from the opposite nature of their trans effects. Thus, while CO binds more strongly to hemes in the presence of a sixth ligand, the repulsive trans effect of NO favors the dissociation of any trans axial ligand to form a 5c-heme complex. Despite this, the majority of hemoproteins actually form 6c-NO complexes due to the tendency of the protein matrix to hold the axial amino acid ligands

(*36*). What are the additional structural factors within hemoproteins which govern 5c-NO formation?

Previous studies have proposed that the ability of hemoproteins to form 5c-NO adducts can be correlated with the strength of their Fe−N(His) proximal bond as indicated by the frequency of the ν(Fe−His) RR vibration in the 5c-ferrous state (*42*). A ν(Fe−His) value of ∼210 cm^{-1} was suggested as the cutoff frequency below which NO is able to cleave the Fe−N(His) bond and above which the Fe−N(His) bond remains intact to form a 6c-NO adduct (*42*). In the case of sGC, the cleavage of the proximal linkage upon reaction with NO has been attributed to a weak Fe−N(His) bond as suggested by the low ν(Fe−His) frequency of ∼204 cm^{-1} (*17*, *18*). A relatively low ν(Fe−His) frequency of 211 cm^{-1} has also been recently determined for a transient 5c form of CooA, generated by photodissociation of the CO adduct (*43*). However, the present study questions the generality of this correlation since *A. xylosoxidans* cyt *c*′ reacts with NO to form a 5c-NO adduct, despite its much higher ν(Fe−His) frequency of 231 cm^{-1}. Furthermore, the similarity in ν(Fe−His) frequencies between cyt *c*′s from different organisms (Table 1) does not account for their different propensities toward forming 5c- vs 6c-NO adducts (*44*). Thus, while cyt *c*′ from *A. xylosoxidans* gives rise to a 5c-NO species, cyt *c*′s from various photosynthetic bacteria give rise to different equilibrium mixtures of 5c- and 6c-NO adducts (*44*).

For both sGC and *A. xylosoxidans* cyt *c*′ it has been observed that reaction of reduced protein with NO initially generates a 6c-NO intermediate which then reacts with an *additional* NO molecule to give the 5c-NO end product (*39*, *45*). Thus, for these proteins it is the properties of the 6c-NO intermediate rather than the 5c-ferrous state which determine whether a 5c-NO adduct is formed. An additional factor favoring the formation of the 5c-NO adduct, suggested by the crystal structure cyt *c*′, is the accessibility of the proximal heme pocket which could allow the His ligand to be displaced by the attack of a second NO molecule directly on the proximal side. Interestingly, the recent X-ray crystal structure of CooA also shows a solvent-exposed His ligand (*12*), although a 6c-NO intermediate has not yet been detected (*19*).

While the tendency of NO and CO to form heme adducts of different coordination number may help to explain the selective influences these two gases on sGC and CooA activity, it may not be the whole story. In the case of CooA, heme coordination number cannot be the sole factor governing enzyme activation since both the inactive ferrous state and activated CO adduct are hexacoordinate. The novel heme coordination chemistry exhibited by cyt *c*′—particularly the ability to bind exogenous ligands from both sides of the porphyrin ring—suggests a new mechanism for ligand discrimination and signal transduction in heme-based sensor proteins. For example, a commonly held view is that activation of sGC by NO is linked to the cleavage of the Fe−N(His) bond upon formation of the 5c-NO adduct and that signal transduction is via conformational changes produced by NO binding to the Fe and remaining on the *distal* side of the heme. However, given the similarities in coordination chemistry between sGC and *A. xylosoxidans* cyt *c*′, could the sGC 5c-NO adduct instead bind NO on the proximal side? Furthermore, could an ability to bind NO and CO to different faces of the heme be a property utilized by sGC and CooA in order to respond differentially to these gases as described above?

Is there any evidence that heme-based gas sensors bind exogenous ligands on different sides of their hemes? X-ray crystal structures of Fe(II)FixL complexed with O_2 and imidazole and Fe(III)FixL reacted with CN^- and NO all show a 6c heme with the exogenous ligand bound at the distal side, although the structure of the 5c-NO adduct of FixL has yet to be determined (*10*, *11*). Although no crystallographic data have been reported for sGC or for ligand adducts of CooA, RR studies of their 5c-NO and 6c-CO adducts provide evidence that within each protein NO and CO bind to the heme in different electrostatic environments (*16*, *19*). Thus, recently published RR studies of sGC_2 indicate a negative heme-pocket polarity for the 6c-CO adduct as opposed to a neutral environment for the 5c-NO species, prompting the authors to propose as one possibility that NO and CO bind to opposite sides of the heme (*16*). In a similar vein, RR spectra of CooA indicate negative heme-pocket polarity for the 6c-CO adduct and a neutral environment for the 5c-NO species (*19*). Interestingly, the recent X-ray crystal structure of ferrous CooA reveals differences in the electrostatic environments around the two faces of the heme, with the Pro 2 ligand surrounded by hydrophobic residues and the His 77 ligand close to the electron-rich sulfur of Cys 75 (*12*). The neutral heme pocket suggested by the RR data of the NO adduct could be explained by NO coordinating at the site originally occupied by Pro 2, whereas the negative polarity implied by the RR data of the CO complex could arise if CO displaced His 77 and interacted with the lone pairs of Cys 75. Evidence that His 77 is displaced in the CO adduct of CooA stems from the apparent loss of imidazolate ligation (attributable to His 77) following CO binding to the ferrous state (*14*). However, a recent time-resolved RR study of photolyzed carbonmonoxy CooA suggests instead that His 77 remains coordinated to the Fe (*43*).

While the RR data of CooA and sGC do not prove that exogenous ligands bind to opposite sides of their hemes, the parallels with the ligand binding and spectroscopic properties of cyt *c*′ suggest that this possibility must be seriously considered. The binding of exogenous ligands to different faces of the heme could help to explain the selective activation responses of CooA and sGC to NO and CO, although it should be pointed out that models for sGC activation must also account for the ability of the xenobiotic, YC-1, to produce activity levels in the 6c-CO adduct comparable with the NO-stimulated enzyme (*41*, *46*, *47*).

In conclusion, the present RR investigation of ferrous, 6c-CO, and 5c-NO forms of *A. xylosoxidans* cyt *c*′ in solution yields structural information on the heme center consistent with the recently reported crystallographic study showing CO bound to the Fe on the distal side of the heme in contrast to NO which exhibits an unprecedented proximal coordination geometry. Our RR studies have particular implications for the mechanisms of ligand selectivity and signal transduction in heme-based sensors. The fact that reduced cyt *c*′ readily forms a 5c-NO complex, despite the high frequency of its ν(Fe−His) vibration, demonstrates that a weak Fe−N(His) bond in the ferrous state is not an absolute requirement for the cleavage of a proximal histidine link upon

binding NO. Furthermore, the ability of cyt *c′* to bind NO and CO on opposite sides of the heme suggests a mechanism for discriminating between different ligand species binding at the heme center. In this regard, it is noted that previously reported RR spectra of sGC as well as CooA are also consistent with different heme environments for CO and NO adducts, suggesting that cyt *c′* may be a useful model for ligand binding in heme-based sensors.

ACKNOWLEDGMENT

We are most grateful to Thomas M. Loehr and Pierre Moënne-Loccoz for helpful discussions and for critically reading the manuscript.

REFERENCES

1. Meyer, T. E., and Kamen, M. D. (1982) *Adv. Protein Chem. 35*, 105−212.
2. Moore, G. R., and Pettigrew, G. W. (1990) *Cytochromes c, Evolutionary, Structural and Physicochemical Aspects*, Springer-Verlag, Berlin.
3. Yoshimura, T., Iwasaki, H., Shidara, S., Suzuki, S., Nakahara, A., and Matsubura, T. (1988) *J. Biochem. 103*, 1016−1019.
4. Yoshimura, T., Shidara, S., Ozaki, T., and Kamada, H. (1993) *Arch. Microbiol. 160*, 498−500.
5. Ferguson, S. J. (1991) *Biochim. Biophys. Acta 1058*, 17−20.
6. Moir, J. W. B. (1999) *Biochim. Biophys. Acta 1430*, 65−72.
7. Cross, R., Aish, J., Paston, S. J., Poole, R. K., and Moir, J. W. B. (2000) *J. Bacteriol. 182*, 1442−1447.
8. Lawson, D. M., Stevenson, C. E. M., Andrew, C. R., and Eady, R. R. (2000) *EMBO J. 19*, 5661−5671.
9. Rodgers, K. R. (1999) *Curr. Opin. Chem. Biol. 3*, 158−167.
10. Gong, W., Hao, B., Mansy, S. S., Gonzalez, G., Gilles-Gonzalez, M. A., and Chan, M. K. (1998) *Proc. Natl. Acd. Sci. U.S.A. 95*, 15177−15182.
11. Gong, W., Hao, B., and Chan, M. K. (2000) *Biochemistry 39*, 3955−3962.
12. Lanzilotta, W. N., Schuller, D. J., Thorsteinsson, M. V., Kerby, R. L., Roberts, G. P., and Poulos, T. L. (2000) *Nat. Struct. Biol. 7*, 876−880.
13. Spiro, T. G., and Li, X. Y. (1988) *Resonance Raman Spectroscopy of Metalloporphyrins*, Vol. 3, John Wiley & Sons, New York.
14. Vogel, K. M., Spiro, T. G., Shelver, D., Thorsteinsson, M. V., and Roberts, G. P. (1999) *Biochemistry 38*, 2679−2687.
15. Fan, B., Gupta, G., Danziger, R. S., Friedman, J., and Rousseau, D. L. (1998) *Biochemistry 37*, 1178−1184.
16. Vogel, K. M., Hu, S., Spiro, T. G., Dierks, E. A., Yu, A. E., and Burstyn, J. N. (1999) *J. Biol. Inorg. Chem. 4*, 804−813.
17. Deinum, G., Stone, J. R., Babcock, G. T., and Marletta, M. A. (1996) *Biochemistry 35*, 1540−1547.
18. Tomita, T., Ogura, T., Tsuyama, S., Imai, Y., and Kitagawa, T. (1997) *Biochemistry 36*, 10155−10160.
19. Reynolds, M. F., Parks, R. B., Burstyn, J. N., Shelver, D., Thorsteinsson, M. V., Kerby, R. L., Roberts, G. P., Vogel, K. M., and Spiro, T. G. (2000) *Biochemistry 39*, 388−396.
20. Ambler, R. P. (1973) *Biochem. J. 1345*, 751−758.
21. Norris, G. E., Anderson, B. F., Baker, E. N., and Rumball, S. V. (1979) *J. Mol. Biol. 135*, 309−312.
22. Cusanovich, M. A., Tedro, S. M., and Kamen, M. D. (1970) *Arch. Biochem. Biophys. 141*, 557−570.
23. Loehr, T. M., and Sanders-Loehr, J. (1993) *Methods Enzymol. 226*, 431−470.
24. Yoshimura, T., Suzuki, S., Nakahara, A., Iwasaki, H., Masuko, M., and Matsubara, T. (1985) *Biochim. Biophys. Acta 831*, 267−274.
25. Strekas, T. C., and Spiro, T. G. (1974) *Biochim. Biohys. Acta 351*, 237−245.
26. Kitagawa, T., Ozaki, Y., Kyooku, Y., and Horio, T. (1977) *Biochim. Biophys. Acta 495*, 1−11.
27. Hobbs, J. D., Larsen, R. W., Meyer, T. E., Hazzard, J. H., Cusanovich, M. A., and Ondrias, M. R. (1990) *Biochemistry 29*, 4166−4174.
28. Othman, S., Richaud, P., Verméglio, A., and Desbois, A. (1996) *Biochemistry 35*, 9224−9234.
29. Bangcharoenpaurpong, O., Schomacker, K. T., and Champion, P. M. (1984) *J. Am. Chem. Soc. 106*, 5688−5698.
30. Smulevich, G., Feis, A., Focardi, C., Tams, J., and Welinder, K. G. (1994) *Biochemistry 33*, 15425−15432.
31. Lawson, D. M., unpublished observation.
32. Moore, G. R., Williams, R. J. P., Peterson, J., Thomson, A. J., and Matthews, F. S. (1985) *Biochim. Biophys. Acta 829*, 83−96.
33. Dobbs, A. J., Anderson, B. F., Faber, H. R., and Baker, E. N. (1996) *Acta Crystallogr. D 52*, 356−368.
34. Iwasaki, H., Yoshimura, T., Suzuki, S., and Shidara, S. (1991) *Biochim. Biophys. Acta 1058*, 79−82.
35. Tomita, T., Hirota, S., Ogura, T., Olson, J. S., and Kitagawa, T. (1999) *J. Phys. Chem. B 103*, 7044−7054.
36. Vogel, K. M., Kozlowski, P. M., Zgierski, M. Z., and Spiro, T. G. (1999) *J. Am. Chem. Soc. 121*, 9915−9921.
37. Li, X. Y., and Spiro, T. G. (1988) *J. Am. Chem. Soc. 110*, 6024−6033.
38. Lukat-Rodgers, G. S., and Rodgers, K. R. (1997) *Biochemistry 36*, 4178−4187.
39. George, S. J., Andrew, C. R., Lawson, D. M., Thorneley, R. N. F., and Eady, R. R. (2001) *J. Am. Chem. Soc.* (submitted for publication).
40. Stone, J. R., and Marletta, M. A. (1995) *Biochemistry 34*, 14668−14674.
41. Friebe, A., Schultz, G., and Koesling, D. (1996) *EMBO J. 24*, 6863−6868.
42. Schelvis, J. P. M., Seibold, S. A., Cerda, J. F., M., G. R., and Babcock, G. T. (2000) *J. Phys. Chem. B 104*, 10844−10850.
43. Uchida, T., Ishikawa, H., Ishimori, K., Morishima, I., Nakajima, H., Aono, S., Mizutani, Y., and Kitagawa, T. (2000) *Biochemistry 39*, 12747−12752.
44. Yoshimura, T., Fujii, S., Kamada, H., Yamaguchi, K., Suzuki, S., Shidara, S., and Takakuwa, S. (1996) *Biochim. Biophys. Acta 1292*, 39−46.
45. Zhao, Y., Brandish, P. E., Ballou, D. P., and Marletta, M. A. (1999) *Proc. Natl. Acad. Sci. U.S.A. 96*, 14753−14758.
46. Stone, J. R., and Marletta, M. A. (1998) *Chem. Biol. 5*, 255−261.
47. Denninger, J. W., Schelvis, J. P. M., Brandish, P. E., Zhao, Y., Babcock, G. T., and Marletta, M. A. (2000) *Biochemistry 39*, 4191−4198.
48. Choi, S., Spiro, T. G., Langry, K. C., Smith, K. M., Budd, D. L., and La Mar, G. N. (1982) *J. Am. Chem. Soc. 104*, 4345−4351.
49. Tamura, K., Nakamura, H., Tanaka, Y., Oue, S., Tsukamoto, K., Nomura, M., Tsuchiya, T., Adachi, S., Takahashi, S., Iizuka, T., and Shiro, Y. (1996) *J. Am. Chem. Soc. 118*, 9434−9435.
50. Teraoka, J., and Kitagawa, T. (1981) *J. Biol. Chem. 256*, 3969−3977.
51. Kim, S., Deinum, G., Gardner, M. T., Marletta, M. A., and Babcock, G. T. (1996) *J. Am. Chem. Soc. 118*, 8769−8770.
52. Miyatake, H., Mukai, M., Adachi, S., Nakamura, H., Tamura, K., Iizuka, T., Shiro, Y., Strange, R. W., and Hasnain, S. S. (1999) *J. Biol. Chem. 274*, 23176−23184.
53. Tsubaki, M., Srivastava, R. B., and Yu, N. T. (1982) *Biochemistry 21*, 1132−1140.
54. Evangelista-Kirkup, R., Smulevich, G., and Spiro, T. G. (1986) *Biochemistry 25*, 4420−4425.
55. Smulevich, G., Evangelista-Kirkup, R., English, A., and Spiro, T. G. (1986) *Biochemistry 25*, 4426−4430.
56. Morikis, D., Champion, P. M., Springer, B. A., and Sligar, S. G. (1989) *Biochemistry 28*, 4791−4800.
57. Biram, D., Garratt, C. J., and Hester, R. E. (1991) in *Spectroscopy of Biological Molecules* (Hester, R. E., and Girling, R. B., Eds.) pp 433−434, Royal Society of Chemistry, Cambridge.

BI0023652